2022

Effect of the Contained Refrigerant Mass on the Efficiency and Effectiveness of Two-phase Heat Exchangers

Christoph Zainer

Kevin Wimmer

Michael Lang

Raimund Almbauer

Effect of the Contained Refrigerant Mass on the Efficiency and Effectiveness of two-phase Heat Exchangers

Christoph ZAINER[1]*, Kevin WIMMER[1], Michael LANG[1], Raimund ALMBAUER[1]

[1]Graz University of Technology,
Institute of Thermodynamics and Sustainable Propulsion Systems,
Inffeldgasse 19, 8010 Graz, Austria
zainer@ivt.tugraz.at
kevin.wimmer@ivt.tugraz.at
lang@ivt.tugraz.at
almbauer@ivt.tugraz.at

* Corresponding Author

ABSTRACT

The development of high-quality, energy-efficient cooling devices requires extensive experience and special knowledge of the individual components and their interaction as an overall system. In refrigeration processes, the heat exchangers (condenser, evaporator) are components that represent a large uncertainty in the modeling and thus probably also a large potential for increasing efficiency.
Up to now, only the total refrigerant charge of the refrigeration cycle is known, but not how it is distributed in the system during operation. Using an internal 1D algorithm for simulating two-phase heat exchangers (1D-HXM), a fin-and-tube condenser operated with R600a is discretized into 100 elements. In the individual elements, the heat flow, thermodynamic state variables and the contained refrigerant mass can be determined.
The performed simulations show that the condenser contains a lot of liquid refrigerant at many operating conditions – i.e. considered over the tube length, they already reach a subcooling state very early. That means that the condenser contains a big amount of the overall refrigerant mass. By now varying the inlet pressure in minimal steps (0.1 bar steps), significant changes of the refrigerant charge in the condenser occur. Therefore, by holding other boundary conditions constant (mass flow R600a and air, …), the contained refrigerant mass in the condenser can be increased or decreased. It can be seen that in a wide range of this pressure variation a subcooling distance of different lengths occurs. The pressure variation thus changes the location of the phase transition in the condenser. However, with large subcooling proportions air outlet temperature and heat output remain nearly unchanged, only the refrigerant mass in the condenser changes. The heat flow and the air outlet temperature remain constant, because the air temperature approaches the subcooled refrigerant temperature and cannot rise any further, while the refrigerant cannot subcool below the air temperature. Therefore, nearly the same amount of heat can be transferred for e.g. 20 elements subcooled and 10 elements subcooled. This means that the entire heat exchanger (HX) is not optimally utilized and in optimal use it can be dimensioned smaller.
The results show that the condenser can contain a large amount of the overall refrigerant mass. By lowering the pressure an optimum condition can be achieved where the condenser is optimally utilized and only a small refrigerant mass is stored (lower condensing pressure means better COP). Further this condition can be used to evaluate and compare different HX designs with each other. Another result is, that for the validation of a HX simulation model, the geometrical position of the phase transition is needed. Moreover, the refrigerant distribution can lead to considerable problems in the behavior of overall cycles with speed-controlled compressors – which could also make an adjustable throttle indispensable for mass removal from the condenser.

1 INTRODUCTION

According to IIR (2019), the refrigeration sector, including air conditioning, claims about 20% percent of the worldwide used elctricity. Since the generation of energy is often associated with significant emissions and greenhouse gases, the development of energy-efficient refrigeration equipment is intended.
Cho *et al.* (2020) shows that a goal of many current studies is to reduce the refrigerant charge of a refrigeration cycle due to its danger of flammability and environmental damage. It is further shown, that large amounts of refrigerant can be stored in the condenser; wherefore the effect of different condenser geometries and refrigerant charges on the

energy consumption are investigated. By, among other things, reducing the condenser length to 70% of the original length, they were able to reduce the refrigerant charge by 14% and see an improvement in energy consumption.
This suggests large uncertainties in the dimensioning of refrigeration cycles by the selection of heat exchangers (condenser, evaporator). Describing the operation of the heat exchangers is not trivial, since the physical processes during the phase transition of the refrigerant are difficult to describe and measure. Therefore, the amount of refrigerant stored in the heat exchangers and its influence on the overall refrigerant distribution as well on the efficiency of the refrigeration cycle are largely unknown. The HX behavior in transient operation is even more difficult to describe because the processes of refrigerant distribution are uncertain. On the one hand, heterogeneous effects occur, and on the other hand, the operation of the used throttle is important. In conventional capillary throttles, the deliverable mass flow is limited by the geometry, and for optimal operation, an appropriate inlet condition must be delivered to the capillary by the condenser. This could make the need for an adjustable throttle for mass redistribution in transient operation indispensable.
Due to the high potential of the heat exchangers to increase efficiency, in this study a simulation model of a fin-and-tube condenser is created with best possible accuracy to analyze the influence of the contained refrigerant mass at different condensing pressures.

2 FIN-AND-TUBE HEAT EXCHANGER

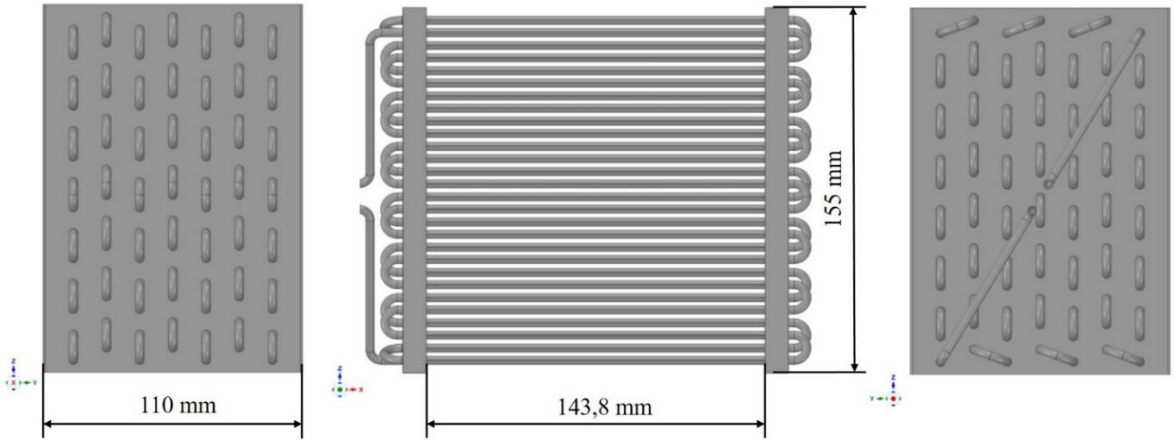

Figure 1: Geometry of the fin-and-tube condenser with main dimensions

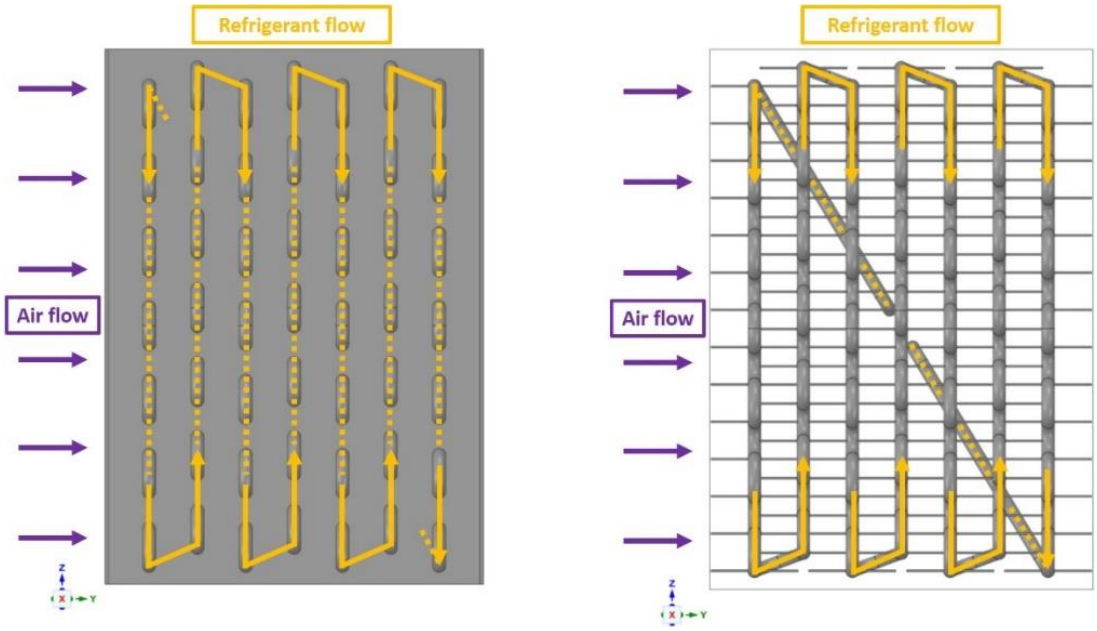

Figure 2: Flow direction of the fluids in the HX (left: with retaining plates; right: without retaining plates)

The geometry and main dimensions of the investigated forced-air fin-and-tube aluminum condenser are shown in detail in Figure 1. The fin-and-tube HX consists of 7 staggered tube rows with 14 tubes each, as well as an inlet and an outlet tube. The tubes result in a total length of $l_{Tube} = 18.375$ m with an inner diameter of $d_i = 2.8$ mm and an outer diameter of $d_o = 3.8$mm. In the main flow cross-section, fixed fins are connected to the 98 straight tube sections. The two retaining plates separate the main flow cross-section from the two U-tube rooms on both sides.
The flow directions of the fluids in the HX is shown in Figure 2. The refrigerant (orange) enters the condenser at the top left and flows through it as shown. The air flow (violet) enters from the left in this view. For a better understanding of the airflow, the HX is also shown without retaining plates.

A dry air volume flow of $\dot{V}_{Air} = 85$ m³/h at an air inlet temperature of $T_{Air,in} = 32$ °C is investigated. The condenser operates with the refrigerant R600a. The superheating temperature of the incoming refrigerant in the HX is determined by the discharge from a fictitious isentropic compressor. The compressor inlet condition is set at $p_{Comp,in} = p_{sat}(-23.3°C) = 0.62939$ bar and $T_{Comp,in} = T_{Air,in} = 32$ °C. Different refrigerant mass flows with different inlet pressures are analyzed in the following.

3 SIMULATION MODEL

To analyze the HX and the amount of refrigerant it contains, a stationary 1D model of the condenser (1D-HXM) is created in MS Excel (Professional Plus 2016 version). The model works with REFPROP substance values (version 9.0) for R600a and thus can also be quickly converted to other refrigerants. Chapter 3.1 shows the discretization procedure and chapter 3.2 the models and correlations used. The assumptions and simplifications made for this purpose, as well as any deviations resulting from them, are given in chapter 0. Chapter 3.4 briefly discusses the validation of the simulation model with comparative values. Finally, in chapter 3.5 a comparison process is defined to make the obtained simulation results comparable with each other.

3.1 Discretization

The geometric discretization is done as best as possible according to the real geometry, where the HX is divided into 100 elements. The inlet and outlet tubes are discretized as separate elements. In between, all 98 tubes in the main flow area including their associated U-tube piece in the U-tube room are defined as separate elements. The element numbering is done according to the refrigerant flow direction and is shown in Figure 3.
Then, for each element, equations are set up to represent the material flows of an element as in Figure 4 and their transferred heat flow between each other. It is important to ensure that the airside of the elements is correctly nested, i.e., for example, the outgoing enthalpy flow of air from E02 is the incoming enthalpy flow in E29. The pipe temperatures are constant for each individual element.

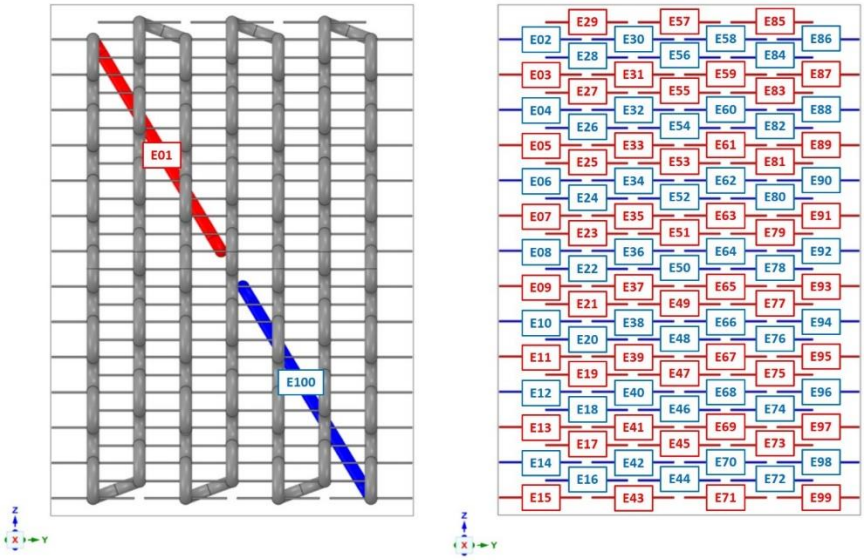

Figure 3: Geometric discretization and element segmentation of the HX

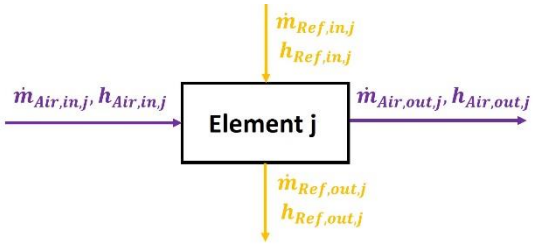

Figure 4: Mass flow and enthalpies of an element j

Under steady-state assumption, the following equations are obtained:

$$\dot{m}_{Ref} h_{Ref,out,j} = \dot{m}_{Ref} h_{Ref,in,j} - \dot{Q}_j \quad (1)$$

$$\dot{m}_{Air} h_{Air,out,j} = \dot{m}_{Air} h_{Air,in,j} + \dot{Q}_j \quad (2)$$

By applying the Upwind-scheme under the assumption of constant tube temperature and perfect heat conduction in the tube applies:

$$\dot{Q}_j = \alpha_{i,j} * A_{i,j} * \left(T_{Ref,in,j} - T_{tube,j}\right) \quad (3)$$

$$\dot{Q}_j = \alpha_{o,j} * A_{o,j} * \left(T_{Tube,j} - T_{Air,in,j}\right) \quad (4)$$

The surface areas $A_{i,j}$ and $A_{o,j}$ of the elements are taken from the geometry. The inner heat transfer coefficient $\alpha_{i,j}$ is calculated from a correlation described in chapter 3.2 and CFD simulations determine the outer $\alpha_{o,j}$. By equating and rearranging equations (3) and (4), the tube temperature $T_{Tube,j}$ can be calculated:

$$T_{Tube,j} = \frac{T_{Air,in,j} + T_{Ref,in,j} * \frac{\alpha_{i,j} * A_{i,j}}{\alpha_{o,j} * A_{o,j}}}{1 + \frac{\alpha_{i,j} * A_{i,j}}{\alpha_{o,j} * A_{o,j}}} \quad (5)$$

Equations (3) and (4) can thus be inserted into equations (1) and (2), after what the outlet enthalpy of the respective element can be calculated.
Together with the pressure loss correlation from chapter 3.2 the outlet states of the elements are determined. Since the air-side pressure drop for such heat exchangers is usually in the order of a few Pascal, it is neglected.

3.2 Correlations and models

To describe the main physical processes in the condenser, correlations for pressure drop and heat transfer coefficients are applied in the 1D model, which are briefly described in this chapter.

3.2.1 Pressure drop

To describe the refrigerant-side pressure drop, the pressure drop correlation according to Müller-Steinhagen and Heck (1986) are incorporated into the 1D-HXM. The model was found on the fluids homepage of Bell (2016-2018) where further literature of the correlation can be found. The model is suitable for vapor quality of 0 to 1 and is easy to integrate.

3.2.2 Refrigerant-side HTC $\alpha_{i,j}$

The refrigerant-side heat transfer coefficient $\alpha_{i,j}$ in the single-phase region (gaseous or liquid) is calculated with a simple HTC correlation for each element j in the respective phase state. The determination of $\alpha_{i,j}$ of the two-phase flow during condensation uses the correlation of Cavallini and Zecchin (1974). This and further literature can be found on the heat transfer homepage of Bell (2016-2019).

3.2.3 Air-side HTC $\alpha_{o,j}$

In order to represent the air-side heat transfer coefficients $\alpha_{o,j}$ of the real flow around the pipe in the best possible way, a 3D-CFD simulation with Ansys Fluent (R2020R2) was carried out to determine them. For each individual tube column a corresponding HTC was calculated and inserted into the simulation.

3.3 Simplifications, assumptions and possible resulting deviations

The 1D model is based on some simplifications and assumptions, which are shown below with possible resulting deviations.

- Airside: The airside flow guidance is not completely correct, as it assumes that the pipes of the pipe rows are one behind the other and not staggered. Furthermore, vertical air mass exchange as well as gravitational influences and buoyancy are not taken into account. In addition, the air-side pressure drop is neglected, since it is in the range of a few Pascal. It should be noted that the heat transfer coefficients determined from the CFD simulation are also based on assumptions and models and deviations may occur here as well.
- Refrigerant-side: The refrigerant side correlations for pressure drop and HTC may give deviations to the real behavior. Other correlations for pressure drop and HTC also lead to different results. It should be noted that the position of the phase transitions - which in turn is related to a correlation for the HTCs - has an influence on the refrigerant-side pressure drop and deviations can result from this. This also applies recursively to the HTC correlation, which change at different pressures.
- Tubes: The assumption of a constant tube temperature per element with perfect heat conduction can lead to deviations, since the temperature of the inner and outer tube walls are not the same in reality. To make this assumption, CFD simulations of the tube elements with fins with conjugate heat transfer (CHT) were performed. The temperature deviations between the inner and outer pipe walls are minimal, which justifies the assumption.
- Neglect of heat conduction in the retaining plates as well as in the outer walls of the fluid domain
- Steady state, homogeneous model: Transient as well as heterogeneous effects such as refrigerant storage in the HX cannot be taken into account with the 1D-HXM.

3.4 Validation

The validation of the 1D model is carried out with comparison values, which are not discussed in more detail here. However, this validation has no comprehensive significance, since only the inlet and outlet states of air and refrigerant are available. The absolute values of the heat flow as well as the inlet and outlet states of air and refrigerant agree well between comparison values and simulation, but an exact validation is not possible due to the unknown geometric position of the phase transition points in the HX. Furthermore, heat conduction as well as heat input via walls may have a significant influence on the comparison values in reality.

3.5 Definition of comparative condenser efficiency ratio

In order to make different operating states of the condenser comparable with each other, a comparison value is defined which is analogous to the COP_h for heat pumps. For this purpose, a fictitious compressor is compressing isentropically from a defined intake state to the respective condenser input state. The condenser efficiency ratio $\zeta_{Cond,s}$ is introduced according to equation (6), which is defined by comparing the dissipated heat flux of the condenser to the isentropic compressor power. The inlet condition to the compressor is defined at $p_{Comp,in} = p_{sat}(-23.3°C) = 0.62939$ bar and $T_{Comp,in} = T_{Air,in} = 32$ °C.

$$\zeta_{Cond,s} = \frac{\dot{Q}_{Cond}}{P_{Comp,s}} = \frac{(h_{Cond,out} - h_{Cond,in})}{(h_{Cond,in} - h_{Comp,in})} \quad (6)$$

4 RESULTS AND DISCUSSION

In the following simulations, the condensing temperature $T_{Ref,Cond}$ is assumed to be the saturation temperature at the inlet pressure $p_{Ref,in}$ of the condenser ($T_{Ref,Cond} = T_{Ref,sat(p_{Ref,in})}$). The inlet pressure is now determined to give a temperature difference $\Delta T_{in} = T_{Ref,Cond} - T_{Air,in}$, where $T_{Air,in} = 32$ °C. In chapter 4.1, the simulation results of a selected operating point are shown and discussed, which will always be referred to in the following ("design operating point"). These simulations are performed in Chapter 4.2 for different refrigerant mass flows $\dot{m}_{Ref}$ (from 0.5 kg/h to 2.5 kg/h). Chapter 4.3 then discusses the lowering of the pressure from the design operating point and chapter 4.4 the pressure increase.

4.1 Temperature profile and heat fluxes of the "design operating point"

Figure 5a) shows the profiles of the refrigerant, tube and entering air temperature of the individual elements at $\Delta T_{in} = 10$ K and a refrigerant mass flow of $\dot{m}_{Ref} = 1.47$ kg/h (refrigerant just condenses completely at this mass flow to $x_{out,E100} = 0$). The superheat section captures about the first seven elements. In the profile of the air temperatures

$T_{Air,in,j}$ of the elements are peaks, which result from the large heat dissipation of the first seven elements (especially element E02) due to the high temperature difference of the superheating section. These temperature peaks are carried on in the upper tubes located one behind the other and can also reverse the direction of the heat flow there, if the refrigerant is already at a lower temperature than the air in this region. Figure 5b) shows the corresponding comparison process (chapter 3.5) in the T-h-diagram and allows the enthalpy differences of compressor and condenser to be read directly. Table 1 shows the results of this operating point, where a comparative condenser efficiency ratio of $\zeta_{Cond,s}$ = 4.12 is obtained. Since the vapor quality at the outlet is at $x_{out,E100}$ = 0, no subcooling occurs ($l_{HX,sub}$ = 0 %) and thus a refrigerant mass of m_{Ref} = 8.9 g is contained in the HX. A pressure drop of Δp_{MSH} = 174 mbar is obtained-

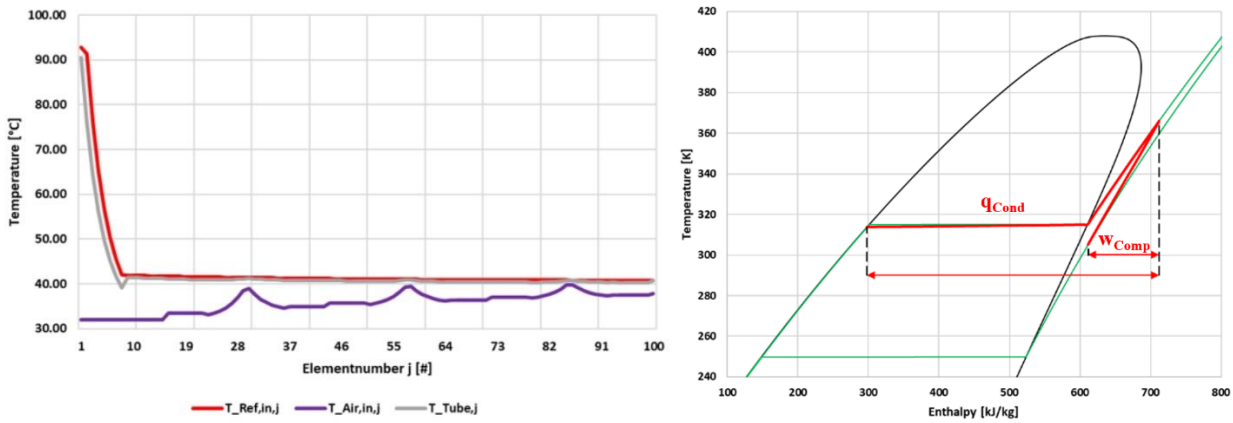

Figure 5: a) (Left) Temperature profile of refrigerant, air and tube in the individual elements j of the condenser at ΔT_{in} = 10 K and $\dot{m}_{Ref}$ = 1.47 kg/h. **b)** (Right) T-h-diagram of corresponding comparison process for $\zeta_{Cond,s}$

Table 1: Results of the design operating point

Δp_{var}	ΔT_{in}	$p_{Ref,in}$	m'_{Ref}	Q'_{cond}	$P_{comp,s}$	$\zeta_{cond,s}$	$x_{out,E100}$	$l_{HX,sub}$	m_{Ref}	Δp_{MSH}
[bar]	[K]	[bar]	[kg/h]	[W]	[W]	[-]	[-]	[%]	[g]	[mbar]
0	10.0	5.60	1.47	169.0	41.1	4.12	0.00	0.0	8.9	174

4.2 Variation of refrigerant mass flow

The above simulation is now performed for different refrigerant mass flows $\dot{m}_{Ref}$ (from 0.5 kg/h to 2.5 kg/h). Figure 6 shows that at a low mass flow rate $\dot{m}_{Ref}$ = 0.5 kg/h a large area of the HX is subcooled ($l_{HX,sub}$ = 78.2 %) and thus a very large mass of refrigerant (m_{Ref} = 49.2 g) is stored. This results in a high $\zeta_{Cond,s}$ = 4.28.

As the mass flow increases up to about $\dot{m}_{Ref}$ = 1.47 kg/h, the heat flux $\dot{Q}_{Cond}$ increases, the stored refrigerant mass as well as the geometric length of the subcooled region decrease and the efficiency $\zeta_{Cond,s}$ decreases slightly but remains almost constant ($\zeta_{Cond,s}$ = 4.12). Reading the values from the diagram at $\dot{m}_{Ref}$ = 1.47 kg/h, we obtain the results of the "design operating point" from chapter 4.1 at which $x_{out,E100}$ = 0.

With further increasing mass flow, the refrigerant exits the HX with a vapor quality bigger than zero ($x_{out,E100}$ > 0), so there is no more complete condensation and thus no more subcooling ($l_{HX,sub}$ = 0 %). The HX can no longer transfer the same amount of heat, which is why the heat flow $\dot{Q}_{Cond}$ decreases. This leads to a significant drop in the condenser efficiency ratio $\zeta_{Cond,s}$. The contained refrigerant mass m_{Ref} is very small due to the low density.

Furthermore, it can be seen that a too low a mass flow is disadvantageous for the overall system, since too much refrigerant is stored in the condenser, which can be missing or needed in the rest of the cycle (e.g. emptying the evaporator). Conventional capillary throttles cannot deliver variable mass flow and are therefore limited to their inlet state, which does not see how much mass is previously stored in the condenser. This can necessitate the need for an adjustable throttle, especially in transient operation where even higher refrigerant displacements occur, to allow efficient operation. Furthermore, a general goal is to keep the amount of refrigerant in the circuit low due to its properties and cost.

Thus, optimal operation of the HX occurs with the maximum possible heat flux $\dot{Q}_{Cond}$ and condenser efficiency ratio $\zeta_{Cond,s}$, and a low stored refrigerant mass m_{Ref}. This suggests that operation near $x_{out,E100}$ = 0 is the optimal operating condition ("design operating point").

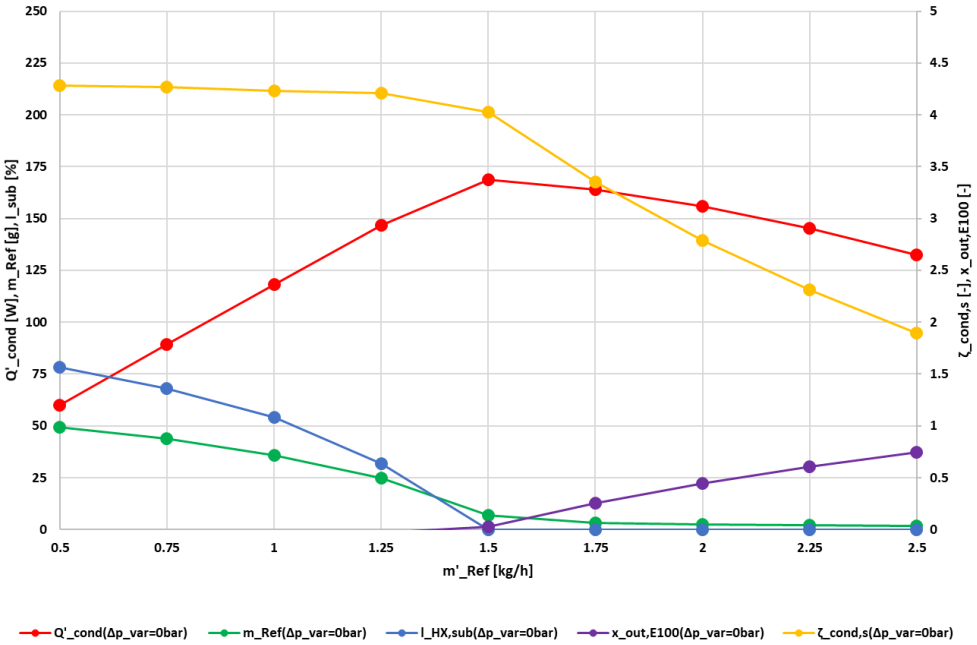

Figure 6: Heat flux $\dot{Q}_{Cond}$, contained refrigerant mass m_{Ref}, percentage of subcooled length of the overall HX-length $l_{HX,sub}$, $\zeta_{Cond,s}$ and $x_{out,E100}$ over the refrigerant mass flow $\dot{m}_{Ref}$ at ΔT_{in} = 10 K

4.3 Pressure reduction

To illustrate the effect of a pressure reduction, the inlet pressure $p_{Ref,in}$ is reduced by Δp_{var} = -0.1 bar (ΔT_{in} = 9.3 K) and Δp_{var} = -0.5 bar (ΔT_{in} = 6.4 K). The variation of the mass flow results in new curves for above variables and are shown together with the profile of the "design operating point" in Figure 7. Table 2 shows the corresponding results of this pressure reduction for the mass flow $\dot{m}_{Ref}$ = 1.47 kg/h.

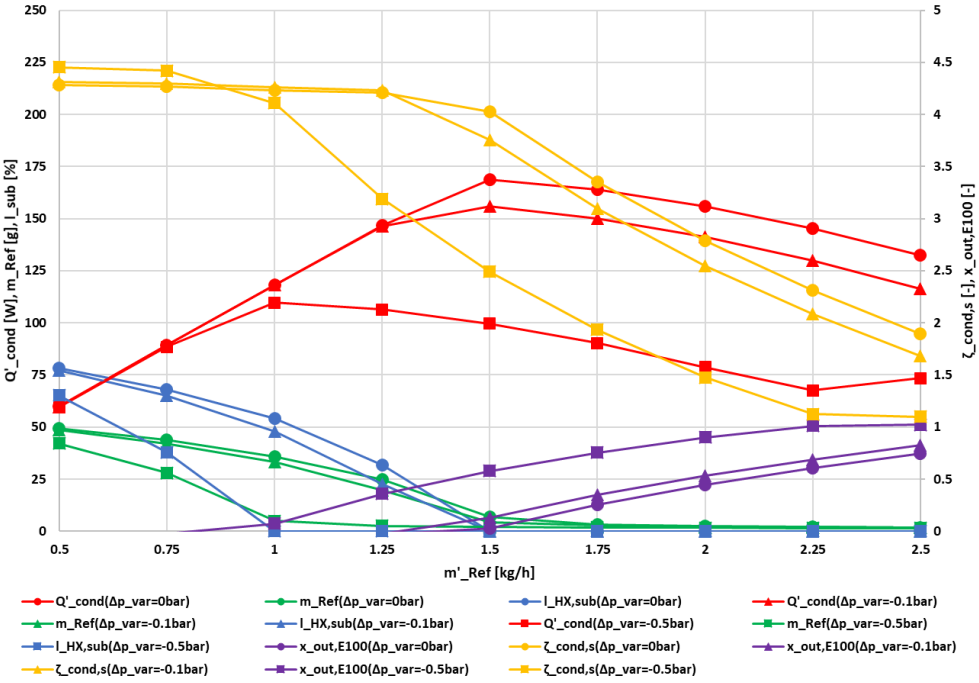

Figure 7: Heat flux $\dot{Q}_{Cond}$, contained refrigerant mass m_{Ref}, percentage of subcooled length of the overall HX-length $l_{HX,sub}$, $\zeta_{Cond,s}$ and $x_{out,E100}$ over the refrigerant mass flow $\dot{m}_{Ref}$ at ΔT_{in} = 10 K (●), ΔT_{in} = 9.3 K (▲) and ΔT_{in} = 6.4 K (■)

With decreasing condensation pressure, the optimum operating point in the diagram shifts to the range of lower mass flows; if the mass flow at the respective ΔT_{in} is increased that $x_{out,E100} = 0$ is exceeded, there is a significant decrease in $\zeta_{Cond,s}$ due to the two-phase condenser exit and thus inefficient utilization of the condenser. The heat flux $\dot{Q}_{Cond}$ drops massively in this range, which is why operation with $x_{out,E100} > 0$ should be avoided in any case.
In the range of lower mass flows than $x_{out,E100} = 0$, the profiles of $\dot{Q}_{Cond}$ and $\zeta_{Cond,s}$ remain almost the same, but the length of the subcooled region as well as the stored refrigerant mass become smaller at lower pressure.
Considering the "design operating point" at $\dot{m}_{Ref}$ = 1.47 kg/h, the heat flow and the efficiency drop massively, as shown in Table 2. A two-phase discharge occurs at the condenser, whereby the stored refrigerant mass in the condenser decreases, but the pressure loss increases massively due to the geometrically greater length of two-phase flow.

Table 2: Results of pressure reduction at $\dot{m}_{Ref}$ = 1.47 kg/h

Δp_{var}	ΔT_{in}	$p_{Ref,in}$	m'_{Ref}	Q'_{cond}	$P_{comp,s}$	$\zeta_{cond,s}$	$x_{out,E100}$	$l_{HX,sub}$	m_{Ref}	Δp_{MSH}
[bar]	[K]	[bar]	[kg/h]	[W]	[W]	[-]	[-]	[%]	[g]	[mbar]
0	10.0	5.60	1.47	169.0	41.1	4.12	0.00	0.0	8.9	174
-0.1	9.3	5.50	1.47	156.5	40.7	3.85	0.10	0.0	4.7	203
-0.5	6.4	5.10	1.47	100.6	39.2	2.56	0.55	0.0	2.1	334

Lowering the pressure while keeping the mass flow constant leads to a massive loss of heat flux and efficiency at the design point. The amount of refrigerant stored decreases, but the pressure drop in the condenser increases significantly.

4.4 Pressure raise

Analogous to the pressure reduction, a pressure increase of $p_{Ref,in}$ by Δp_{var} = + 0.1 bar (ΔT_{in} = 10.7 K) and Δp_{var} = + 0.5 bar (ΔT_{in} = 13.3 K) is performed and shown in Figure 8.

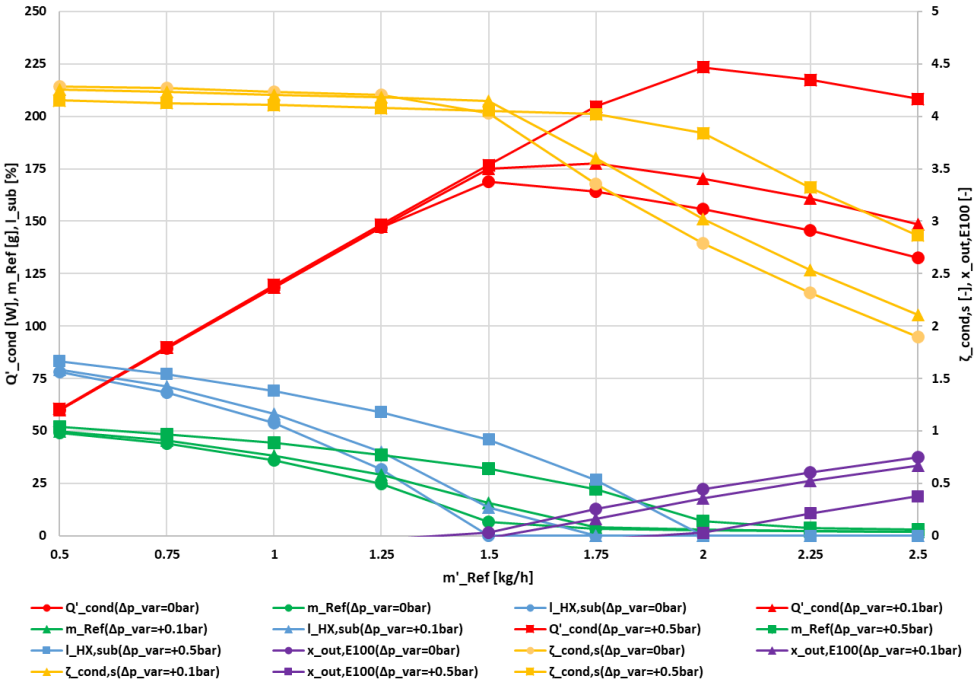

Figure 8: Heat flux $\dot{Q}_{Cond}$, contained refrigerant mass m_{Ref}, percentage of subcooled length of the overall HX-length $l_{HX,sub}$, $\zeta_{Cond,s}$ and $x_{out,E100}$ over the refrigerant mass flow $\dot{m}_{Ref}$ at ΔT_{in} = 10 K (●), ΔT_{in} = 10.7 K (▲) and ΔT_{in} = 13.3 K (■)

Increasing the condensation pressure has exactly the opposite effect as shown in chapter 4.3. The optimum operating points ($x_{out,E100} = 0$) shift to areas of greater mass flow. At higher pressure, the same or a larger (at large mass flow) amount of heat can be transferred at a high efficiency $\zeta_{Cond,s}$. At the same time, however, more mass is stored in the condenser and thus the subcooling distance is geometrically longer. At higher pressure, $x_{out,E100} = 0$ is exceeded only at a very high mass flow, after which the behavior of the HX becomes inefficient again.

Based on the "design operating point" from chapter 4.1 at $\dot{m}_{Ref}$ = 1.47 kg/h, as shown in Table 3, the transferred heat flux increases slightly because a small amount of heat capacity flux can still be delivered to the air for subcooling the refrigerant. The compressor power increases due to the compression to a higher pressure level, which leads to a nearly constant $\zeta_{Cond,s}$ for the mentioned pressure increases. However, without a significant change in heat flux and $\zeta_{Cond,s}$, there is a massive increase in the amount of refrigerant stored in the HX and the geometric length of the subcooling path. The pressure drop decreases due to the large fraction of single-phase flow in the condenser.

Table 3: Results of pressure raise at $\dot{m}_{Ref}$ = 1.47 kg/h

Δp_{var}	ΔT_{in}	$p_{Ref,in}$	m'_{Ref}	Q'_{cond}	$P_{comp,s}$	$\zeta_{cond,s}$	$x_{out,E100}$	$l_{HX,sub}$	m_{Ref}	Δp_{MSH}
[bar]	**[K]**	**[bar]**	**[kg/h]**	**[W]**	**[W]**	**[-]**	**[-]**	**[%]**	**[g]**	**[mbar]**
0	10.0	5.60	1.47	169.0	41.1	4.12	0.00	0.0	8.9	174
+0.1	10.7	5.70	1.47	171.9	41.4	4.15	sub	18.6	17.8	151
+0.5	13.3	6.10	1.47	173.4	42.8	4.06	sub	47.9	32.7	102

This means that when the pressure is increased, there is no improvement in efficiency or a significant bigger heat flux at the same mass flow rate; however, the amount of refrigerant stored increases massively with rising pressure.

5 CONCLUSION

The results show that at minimum pressure differences the condenser can store a significant amount of refrigerant or operate very inefficient. If the pressure is increased further, there is no significant increase in heat flux or improvement in efficiency when the mass flow rate remains the same; however, the condenser begins to store a large amount of refrigerant. When the pressure is lowered, both the heat flux and efficiency decrease significantly and the pressure drop increases sharply. This shows that the geometrical transition points of the phase transitions in the heat exchangers are of significant importance. Thus, the optimum operation of the condenser is when the refrigerant is just fully condensed at the outlet (x_{out} = 0)

In optimal condenser operation (x_{out} = 0), almost the largest possible heat flux is transferred with very good efficiency and a low stored refrigerant mass, what allows a reduction of the amount of refrigerant in the overall cycle by optimal condenser operation.

The simulations can be performed for different ΔT_{in}, air flow rates $\dot{V}_{Air}$ and air inlet temperatures $T_{Air,in}$, and thus characteristic diagrams can be generated. These maps can be used to determine the optimum operating points of the condenser under the respective conditions. If these maps are also created for the evaporator, it is possible to find conditions with optimal operation here as well. By matching the condenser and evaporator, the best possible efficiency of the heat exchangers can be achieved in optimum operation, and the refrigerant charge of the circuit can be significantly reduced. This can be achieved, e.g., by comprehensive control, which might require an adjustable throttle for controlled mass removal from the condenser. Especially in transient operation, the storage of refrigerant in the condenser can be a disadvantage, since conventional capillary throttles are limited in their flow state due to their geometry and may not be able to optimally perform the distribution of refrigerant in the overall cycle.

Furthermore, these maps can be used for the comparison and evaluation of different HX designs and thus support the development process of new refrigeration circuits.

6 NOMENCLATURE

Abbreviations		h	Enthalpy	Comp	Compressor
1D	One dimensional	l	Length	Cond	Condenser
3D	Three dimensional	m	Mass	h	Heating
CFD	Computational fluid dynamics	m'	Mass flow	HX	Heat exchanger
CHT	Conjugate heat transfer	p	Pressure	i	Inner
COP	Coefficient of performance	P	Power	in	Inlet
COPh	Coefficient of performance for heating	q	Specific heat	j	Count variable (element number)
HTC	Heat transfer coefficient	Q'	Heat flux	o	Outer
HX	Heat exchanger	T	Temperature	out	Outlet
HXM	Heat exchanger model	V'	Volume flow	Ref	Refrigerant
MS	Microsoft	x	Vapor quality	s	Isentropic
MSH	Müller-Steinhagen and Heck	**Greek symbols**		sat	Saturation
R600a	Isobutane	α	Heat transfer coefficient	sub	Subcooled
Roman symbols		Δ	Delta (Difference)	Tube	Tube
A	Area	ζ	Condenser efficiency ratio	var	Variation
d	Diameter	**Subscripts**			
E	Element	Air	Air		

7 REFERENCES

Bell, C., 2016-2018. fluids: Fluid dynamics component of Chemical Engineering Design Library (ChEDL) https://github.com/CalebBell/fluids.

Bell, C., 2016-2019. ht: Heat transfer component of Chemical Engineering Design Library (ChEDL) https://github.com/CalebBell/ht.

Cavallini, A., Zecchin, R., 1974. A dimensionless correlation for heat transfer in forced convection condensation. 5th International Heat Transfer Conference, Tokyo, Japan, 309-313. doi: 10.1615/IHTC5.1220

Cho, W., Jang, D., Lee, S., Yun, S., Kim, Y., 2020. Refrigerant charge reduction in R600a domestic refrigerator-freezer by optimizing hot-wall condenser geometry. International Journal of Refrigeration, Volume 117, 295-306, doi: 10.1016/j.ijrefrig.2020.05.012.

IIR, 2019. The role of refrigeration in the global economy. 38th Note on Refrigeration Technologies, https://iifiir.org/en/fridoc/142028, doi: 10.18462/iif.NItec38.06.2019

Müller-Steinhagen, H., Heck, K., 1986. A Simple Friction Pressure Drop Correlation for Two-Phase Flow in Pipes. Chemical Engineering and Processing: Process Intensification 20, no. 6, 297-308. doi:10.1016/0255-2701(86)80008-3.

8 ACKNOWLEDGEMENT

This research was created in HexTraSim, a research project supported by the Austrian Research Promotion Agency (FFG) under the reference number 883663 and by Liebherr-Hausgeräte Lienz GmbH.